Rijks*universiteit* Groningen | Faculteit der Wiskunde en Natuurkunde
Technische Natuurkunde | *Onderzoeksgroep:* Fysica van Nanodevices

Electronic detection study of magnetization dynamics in ferromagnetic/nonmagnetic systems

Master thesis by:

Maksym Sladkov

Group Leader: Prof. Dr. Ir. B. J. van Wees

Supervisor: Ir. M. V. Costache

Referent: Prof. Dr. Ir. P. van Loosdrecht

Period: September 2005 - July 2006

Credits: 54 ECTS

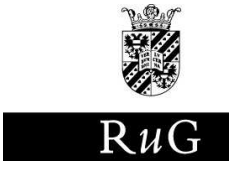

.

Abstract

Latest research in a field of spintronics has shown strong mutual interaction between magnetization dynamics and spin polarized electronic transport. A spin polarized current can drive magnetization dynamics, while resonant magnetization dynamics can lead to generation of the spin current. The first effect is originated due to the spin torque mechanism, while the second one is related to the spin pump effect. In fact these two effects are of the same nature and are strongly depended on the properties of interface between ferromagnetic and paramagnetic metals.

In this work we study magnetization dynamics of mesoscopic ferromagnetic strip which is contacted by paramagnetic metals. Two experiments are reported. In a first one we show the applicability of the coplanar strip waveguide for driving and electrical detecting the uniform precession mode of the ferromagnetic resonance in an on-chip device with a micrometer sized ferromagnetic strip. The second experiment was designed for estimation of the magnetization precession amplitude. We have utilized effect of anisotropic magneto resistance, which is, for our knowledge, the first experiment of this type on a submicron ferromagnetic particle in a coplanar spintronics device.

In addition, theoretical analysis of the uniform magnetization dynamics has been made with a brief inside into nonuniform effects e.g. spin wave generation.

We have also estimated the effect of the spin pumping in our devices by analyzing existing theoretical models which are describing this phenomena.

Contents

Chapter 1

Introduction to spintronics and magnetoelectronics

Since the discovery of Giant Magneto Resistance (GMR) effect [1], transport properties of ferromagnetic (FM) materials, as well as FM/NM (normal metal) interfaces are attracting a lot of attention. The main reason for that is a strong coupling between charge transport and spin transport in FM, which can open a way for creating new type of devices and combine functionality of pure electrical and pure magnetic effects resulting in a new field of physics known as the "spintronics" or "magnetoelectronics" [2].

Back in 1936 Mott provided a pioneering idea which become the basis for a spin dependent transport [3]. He realized that when the spin flip processes are not strong enough the antiparallel with respect to the spin degree of freedom electron states do not mix during the scattering processes. In easy words, electronic transport in ferromagnets is spin polarized. Later, this has been developed into a comprehensive spin transport model, which provides an explanation for a various of magnetoresistive phenomena known as Valet and Fert "two current model" [4].

The phenomena of spin polarized current has a close relation to the operation of GMR devices [1], which consists of sandwich-like structure, where two ferromagnets (FM) are separated by a layer of paramagnetic metal (NM).Two types of GMR structures can be distinguished: current flows parallel (CIP, current in plane) or perpendicular (CPP, current perpendicular to the plane) to the interfaces between the different layers, as depicted in Fig.1.1.

In both geometries, the resistance depends on the relative orientation of the magnetizations M_1 and M_2, which is generally called "spin valve effect" [5]. The functionality of the GMR structure can be simply characterized, when one is talking about CPP geometry, however, the physics which stands behind the CIP geometry is not much different.

The key ingredients for the GMR devices are the large spin polariza-

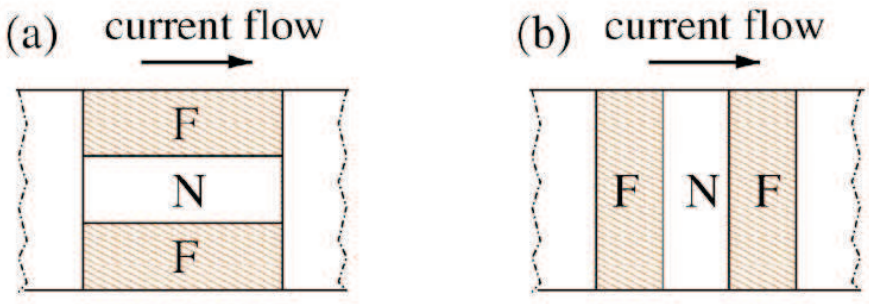

Figure 1.1: Schematic illustration of (a) the current in plane (CIP), (b) the current perpendicular to the plane (CPP) giant magnetoresistance geometry [2].

tion of the current and the ability to control the relative orientation of the magnetization in ferromagnetic layers.

The confirmation of spin polarization of the current which flows through the FM/NM interface was shown by Jedema *et. al.* [6]. The authors were able to detect the pure spin current by separating it from a charge current using the spin valve geometry, which become known as a non-local spin detection.

It was actually shown that dynamics of magnetization in ferromagnetic layers and effect of spin polarization of the current has a strong impact on each other. Berger [7] and Slonczewski [8] independently predicted that spin current can induce a torque on magnetization of ferromagnet. This was experimentally demonstrated by Tsoi *et. al.*[9] as a magnetization precession driven by spin polarized current in $(Co/Cu)_N$ multilayers, whereas Myers *et. al.*[10] observed switching of the orientation of magnetic moment by perpendicular electric current in $Co/Cu/Co$ sandwich. Much earlier, a coupling between a dynamic ferromagnetic magnetization and spin accumulation in adjacent normal metals has been postulated by Janossy and Monod [11] and Silsbee *et. al.* [12].

The effect of the spin transport on magnetization dynamics was shown by Mizukami *et. al* [13], in an experiment on ferromagnetic resonance in a FM/NM sandwich, where the influence of the spin flip rate in a NM on a line width of the resonance has been demonstrated.

Recently, a theoretical model which describes the coupling between magnetization dynamics and spin transport was developed by group of Gerrit Bauer in Delft University of Technology. They predict that resonance precession of ferromagnetic magnetization can induce spin current flow from FM into NM. This effect got a name "spin pumping" and explains results

of Mizukami's experiment as an angular momentum loss of the FM due to injection of the spins into adjacent NM.

The spin pumping effect provides a possibility to create a source of pure spin current - spin battery, where a ferromagnet under resonance magnetization precession will emit spins into an adjacent conductor. The pure spin current can be used for reversing magnetization of another ferromagnet according to the spin torque mechanism [8, 7].

All the effects described above can be generally called "nonlocal magnetization dynamics". A comprehensive review of this phenomena is written by Tserkovnyak *et. al.* [14].

In this work the main focus is to study the dynamics of ferromagnetic magnetization by means of electrical detection, with the ultimate goal of creating a spin battery. The theoretical aspects of ferromagnetic resonance are written with reference mainly to Gurevich and Melkov [15] and are presented in Chapter 2. Chapter 3 is devoted to experiments on detecting ferromagnetic resonance (FMR) of submicron sized permalloy strip using magnetic flux pick-up method. In Chapter 4 experiments on detecting FMR using the AMR (the anomalous magneto resistance) effect are shown. Chapter 5 analyzes the existing models for spin battery [16, 17]. The last chapter is devoted to the basic concepts of the spin waves physics, which could play an important role in nonlocal effects driven by magnetization dynamics.

Chapter 2

Uniform dynamics of ferromagnetic magnetization

2.1 Equation of motion for vector of magnetization

In order to describe the dynamics of ferromagnetic magnetization it is usually not necessary to consider the microscopic picture of ferromagnet. It is more convenient to describe the magnetic state of the FM by introducing the so-called macro-spin $\vec{M}$, which is defined as the total magnetic moment per unit volume. Below the Curie temperature the magnitude of $\vec{M}$ is equal to the saturation magnetization M_s, which for bulk permalloy ($Py = Ni_{80}Fe_{20}$) is $\mu_0 M_s \simeq 1\ T$. An applied magnetic field $\vec{H}$ exerts a torque on $\vec{M}$, resulting in precessional motion of the magnetization (Fig.2.1):

$$\frac{d\vec{M}}{dt} = -\gamma \vec{M} \times \vec{H} \tag{2.1}$$

where $\gamma = g\mu_B/\hbar$ is the gyromagnetic ratio, which can vary for different materials since it also includes the orbital motion contribution to the magnetization. For permalloy, γ has the value 176 GHz/T.

An important property of equation (2.1) is that it conserves the modulus of the vector of magnetization, which reflects our approximation of the macro-spin model.

The solution of the torque equation (2.1) is the vector, which is precessing around the direction of effective magnetic field. When the system obeys spherical symmetry, vector $\vec{M}$ is drawing the circle (circular precession), in other cases the trajectory is more complicated. In this work, the main attention will be paid to the elliptical precession, which is common for ferromagnetic thin films and strips.

2.2 Damping of the precessional motion

The equation of motion (2.1) for the magnetization is valid only in the ideal case, when energy of the precessional motion does not dissipate. In reality there are a number of dissipation mechanisms, such as thermal motion of the crystal lattice, spin-orbit interaction, magnetic inhomogeneity of sample and applied field, spin diffusion into adjoined metal, and so on.

A way to include dissipation was suggested by Landau and Lifshitz [18] by introducing a phenomenological parameter of dissipation λ, resulting in:

$$\frac{d\vec{M}}{dt} = -\gamma\vec{M} \times \vec{H} - \frac{\gamma\lambda}{M_s^2}\vec{M} \times (\vec{M} \times \vec{H}) \tag{2.2}$$

where the first term is as before, while the second term accounts for dissipation.

A more simplified equation was suggested by Gilbert [19], in which the product $\vec{M} \times \vec{H}$ was approximately replaced by $-\gamma^{-1}\partial\vec{M}/\partial t$ in dissipation term. A new dimensionless damping parameter $\alpha = -\lambda/M_s$ was introduced , known as the Gilbert damping parameter, resulting in a well known Landau-Lifshitz-Gilbert (LLG) equation:

$$\frac{d\vec{M}}{dt} = -\gamma\vec{M} \times \vec{H} + \frac{\alpha}{M_s}\vec{M} \times \frac{d\vec{M}}{dt} \tag{2.3}$$

The last equation describes the dissipation as a some sort of "friction force" which is proportional to the rate of changing of the $\vec{M}$. It can be easily checked that eq.(2.3) is different from eq.(2.2) only in second order of α, which is negligible since typical range for α is $10^{-2}..10^{-3}$.

It is important to note that in frame of macro-spin approach, dissipation leads only to the damping of the precession cone angle, while magnitude of the $\vec{M}$ remains constant. The LLG model, indeed, satisfies this condition.

2.3 Magnetization dynamics of a thin film

In order to describe the motion of the magnetization in a thin film, one has to solve the LLG equation including the shape anisotropy, which results in elliptical rather than circular precessional motion of the magnetization.

Let's consider the tangentially (in-plane) magnetized thin film (Fig.2.1). The film is assumed to be a single domain with a saturation magnetization M_s.

The external bias magnetic field $\vec{H}_0$ is also applied in-plane, while the driving radio frequency field $h_{rf}(t)$ is applied in the out-of-plane direction. Since the thickness of the film is much smaller than the lateral sizes, only the out-of-plane demagnetization field must be taken into account [20], resulting

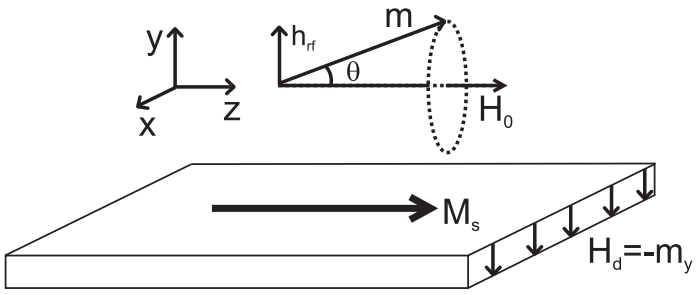

Figure 2.1: Schematic illustration of magnetization precession in a FM thin film. The demagnetizing field H_d exists only in the $\vec{y}$ direction and opposes m_y magnetization.

in an effective magnetic field inside the film $\vec{H}(t) = [-N_y m_y(t) + h_{rf}(t)] \cdot \vec{y} + H_0 \cdot \vec{z}$, where N_y is the out-of-plane demagnetizing factor, which is in our case approximately equal to 1.

The magnetization vector can be written as $\vec{M}(t) = m_x(t) \cdot \vec{x} + m_y(t) \cdot \vec{y} + M_s \cdot \vec{z}$, where it is assumed that angle of precession is small, resulting in unchanged magnetization along the $\vec{z}$ direction.

It is convenient to solve LLG equation in terms of complex amplitudes. For those we assume the circular polarization of the driving rf field $h_{rf}(t) = h_0 e^{i\omega t}$ and the *ansatz* solution for the LLG equation (2.3) will be $m_{x,y}(t) = m_{x,y} e^{i\omega t}$. [1] Later, the real solutions for the time dependent magnetization can be found as $m_{x,y}(t) = Re[m_{x,y} e^{i\omega t}]$. This will give response of the system on a driving field of the form $h_{rf}(t) = h_0 cos\omega t$.

For small angle precession, the LLG equation can be linearized in vicinity of equilibrium state, which corresponds to magnetization vector aligned along the $\vec{z}$ direction, namely $\partial m_z / \partial t = 0$.

Substitution of the $\vec{M}(t)$ and $\vec{H}(t)$ into LLG equation and further neglecting of all the quadratic terms and cross-products of h_0, m_x and m_y leads to the following system of algebraic linear equations:

$$\begin{aligned} i\omega m_x &= -\gamma (H_0 + M_s) m_y + \gamma M_s h_0 + i\omega\alpha m_y \\ i\omega m_y &= -\gamma H_0 m_x - i\omega\alpha m_x \end{aligned} \tag{2.4}$$

In order to find the eigenfrequency of the magnetization precession, we set $h_0 = 0$, then a nontrivial solution will exist only when the determinant

[1] The requirement of the circular polarization of the rf field in general is not necessary since the linearly polarized field can be presented as a superposition of right and left circular polarizations. Then, coordinate transformation into rotation frame and rotation wave approximation (RWA) allows to consider only one circular polarization [21].

of the system is equal to 0. This condition gives us the eigenfrequency of the precession:

$$\omega_0^2 = \gamma^2 H_0 \left(H_0 + M_s\right) \tag{2.5}$$

where all the terms quadratic in α were neglected. Eq.(2.5) gives the frequency of the ferromagnetic resonance (FMR) in a thin film and is an extreme case of the famous Kittel's equation for the FMR of the ferromagnetic ellipsoid [20].

2.4 Frequency dependence of the magnetic susceptibility

When eigenfrequency of the ferromagnetic precession is found the solution of the LLG equation for the vector of magnetization $\vec{M}(t)$ can be written.

Since the LLG equation assumed to be linear, the solution for time dependent magnetization $\vec{m} = m_x(t) \cdot \vec{x} + m_y(t) \cdot \vec{y}$ will have a form:

$$\begin{aligned} m_x &= \chi_T(\omega, \omega_0) h_{rf}(\omega) \\ m_y &= \chi_L(\omega, \omega_0) h_{rf}(\omega) \end{aligned} \tag{2.6}$$

Using relation (2.6) the solution of the equation (2.4) can be written as:

$$\chi_L\left(\omega\right) = -\gamma M_s \frac{\gamma H_0 + i\omega\alpha}{\omega^2 - \omega_0^2 - i\omega\alpha\gamma\left(2H_0 + M_s\right)} \tag{2.7}$$

$$\chi_T\left(\omega\right) = \gamma M_s \frac{i\omega}{\omega^2 - \omega_0^2 - i\omega\alpha\gamma\left(2H_0 + M_s\right)} \tag{2.8}$$

were ω_0 is the FMR frequency given by Eq.(2.5), index L stays for $\vec{y}$ direction and reflects longitudinal magnetization response on the driving field, while index T defines $\vec{x}$ direction, which is transverse to the polarization of the rf field.

Both the transverse and longitudinal susceptibilities have a pole when $\omega = \omega_0$. The behavior of the susceptibility as a function of the applied magnetic field is shown in Fig.(2.2). Since the susceptibility is a complex function it is useful to note, that imaginary part responsible for energy which is absorbed by precessing magnetization, while real part is a dispersive component and relevant to the group velocity of the propagation of electromagnetic waves through the FM.

The amplitude of the ferromagnetic precession, which is usually expressed in terms of the precession cone angle $\theta = \chi_{T,L} h_0 / M_s$ can be much larger than the amplitude of the driving field (in terms of cone angle h_0/M_s),

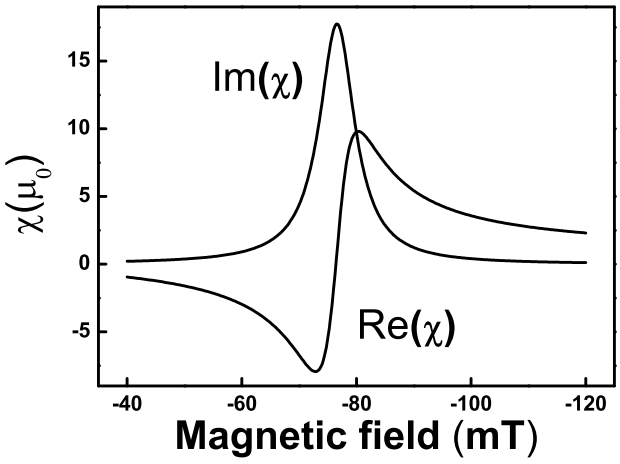

Figure 2.2: Real and imaginary parts of longitudinal high frequency magnetic susceptibility $\chi_L(\omega)$ as a function of applied magnetic filed for an 8 GHz driving field and Gilbert damping parameter $\alpha = 0.015$.

which is a signature of the fact that magnetization is precessing in resonance (coherently) with an rf-field. In other words, after switching on the rf-field, the energy which is absorbed by the system during one period of the precession is larger than the energy dissipation caused by damping processes. Since the dissipation term in the LLG equation (2.3) is proportional to the amplitude of precession, the settled amplitude will be finite and defined by h_0 and α.

Time dependence of the x and y projections of magnetization as a response to the driving field $h_{rf}(t) = h_0 cos\omega t$ are shown at fig.2.3 for the resonance at 8 GHz. The real amplitude of m_x, m_y and h_rf are given in terms of θ-angle of precession.

As was mentioned before, magnetization precession in a thin film is not spherical, but elliptical, where the elipticity is caused by the presence of a demagnetizing field in the $\vec{y}$ direction. The expressions for the magnetic susceptibility allows us to find the ellipticity parameter at resonance, which is:

$$\xi = \frac{\chi_L}{\chi_T}_{\ at\ \omega=\omega_0} = \sqrt{\frac{H_0}{H_0 + M_s}} \tag{2.9}$$

Sweeping either the bias magnetic field or the frequency of the driving field through the resonance does not change the elipticity of precession only

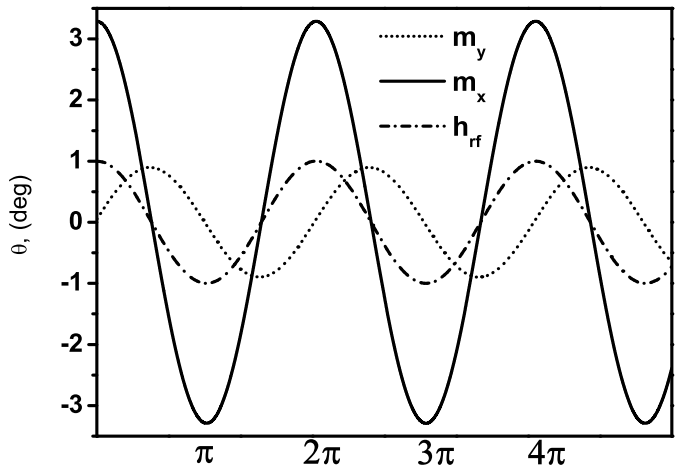

Figure 2.3: Time dependence of the x and y projections of the magnetization for the resonance at 8 GHz driving field and Gilbert damping parameter $\alpha = 0.015$.

the amplitude.

2.5 Magnetization dynamics of a ferromagnetic strip

In a FM strip the demagnetizing field must be accounted for in two directions, namely in $\vec{y}$ and $\vec{x}$, if the strip is elongated in the $\vec{z}$ direction.

By following the same procedure as for the thin film, one can find the FMR dispersion law and the frequency dependence of magnetic susceptibility.

For a bias magnetic field applied along the $\vec{z}$ direction, the magnetization vector is written as $\vec{M}(t) = (m_x(t), m_y(t), M_s)$. The effective magnetic field will have the form $\vec{H}_{eff} = (-N_x m_x, h_0 - N_y m_y, H_0 + H_{an})$ for a driving rf-field linearly polarized in the $\vec{y}$-direction. An additional anisotropy field H_{an} has been introduced in order to account, if necessary, for crystalline anisotropy, remanent magnetization, *etc.*, and N_x and N_y are demagnetizing factors of the strip as calculated in [22].

Under the above conditions, the FMR dispersion takes the following form:

$$\omega_0^2 = \gamma^2 (H_0 + H_{an} + N_x M_s)(H_0 + H_{an} + N_y M_s) \tag{2.10}$$

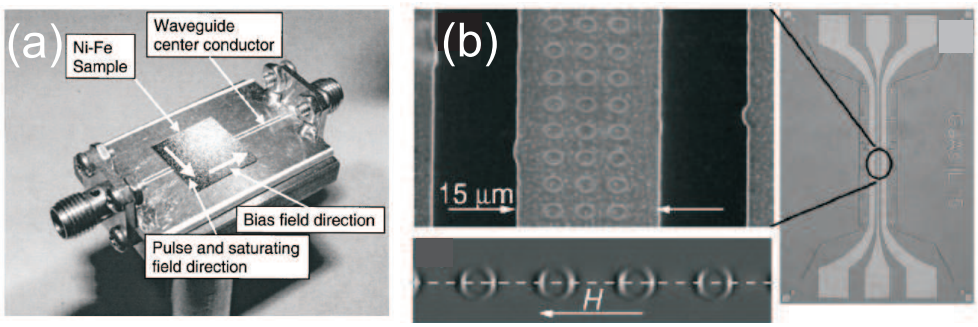

Figure 2.4: (a)Photograph of coplanar waveguide (CPW) used in the Pulsed Inductive Microwave Magnetometer (PIMM) system [28]. (b) Optical micrograph of the CPW used in measuring of resonance absorption of ferromagnetic rings [26]

and the frequency dependence of the susceptibility is as follows:

$$\chi_L(\omega) = -\gamma M_s \frac{\gamma(H_0 + H_{an} + N_x M_s) + i\omega\alpha}{\omega^2 - \omega_0^2 - i\omega\alpha\gamma\,(2(H_0 + H_{an}) + M_s)} \tag{2.11}$$

$$\chi_T(\omega) = \gamma M_s \frac{i\omega}{\omega^2 - \omega_0^2 - i\omega\alpha\gamma\,(2(H_0 + H_{an}) + M_s)} \tag{2.12}$$

2.6 FMR experiments

Ferromagnetic resonance allows us to study not only the magnetization dynamics, but also properties of the FM material, such as the saturation magnetization M_s, anisotropy field, gyromagnetic ratio γ and Gilbert damping parameter α.

FMR experiments date back to the early 50's. At that time, FMR detection was based on the power absorption technique, in which bulk piece of ferromagnet was embedded in a microwave cavity and positioned in a bias magnetic field [23]. A modern variation on this technique for studying the magnetization dynamics of thin ferromagnetic films or ensembles of ferromagnetic micro-particles is to use coplanar waveguide (CPW) [24] with the ferromagnetic material on top of it [25, 26, 27], (Fig.2.4).

The next family of FMR experiments is based on the detection of the magnetic flux, which is created by the motion of the vector of magnetization. Here, the method is based either on the direct detection of a flux by positioning inductive pick-up coil close to the ferromagnet, or by sensing the modified inductance of the CPW, which is filled with ferromagnetic material [29, 30].

Recently, a few more techniques have been reported. Among them are FMR detection by using anomalous magneto resistance (AMR) effect, in which the resistance of the ferromagnet depends on the relative orientation between the magnetization and the direction of current flow [31, 32] and magnetic flux detection using a superconducting quantum interference device (SQUID) [33, 34].

Chapter 3

On-chip detection of ferromagnetic resonance of a single submicron permalloy strip

3.1 Aim of the experiment

Experiments on spin pumping (Chapter 4 of this thesis) requires uniform precession of magnetization of small ferromagnetic particle. Another requirement is a large cone angle of that precession, which can be provided by spatially localized high intensity rf magnetic field.

The devices presented in this experiment were designed to study the cross-talk between two coplanar strip wave guides (CSW) in a close proximity, in which one wave guide is used to drive a high amplitude, localized rf-field, and the second one to detect it. We use a magnetic flux pick-up detection method for performing a highly sensitive FMR experiment on an individual submicrometer size ferromagnetic strip. We show that FM strip can be driven in a uniform magnetization precession mode.

3.2 Device fabrication and measurement techniques

Fig.3.1(a) shows a schematic illustration of the device used in this study, while the scanning electron microscope picture of the central region of the device which contains a ferromagnetic strip is presented in Fig.3.1(b). The permalloy ($Py = Ni_{80}Fe_{20}$) strip is positioned at 2.5 μm distance from the shorted-end of a CSW on the left side of the sample and connected with the copper (Cu) leads to another CSW on the right side (Fig.3.1(a)). The CSW

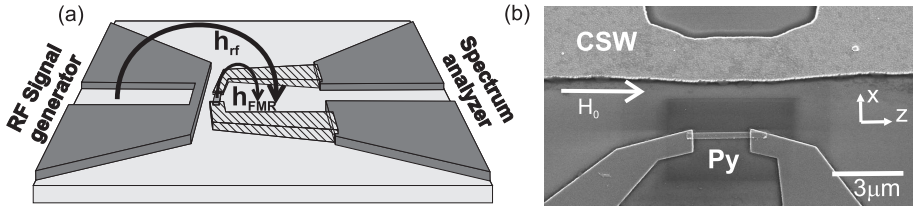

Figure 3.1: (a) Schematic diagram of the device used in experiment. On the left side the rf current passes through the shorted-end of the coplanar strip and generates an rf magnetic field h_{rf} according to the Biot-Savart law. The magnetization precession in the Py strip at resonance induces a magnetic field h_{FMR}. The pick-up ac voltage is measured using the coplanar strip situated at the right side of the device connected to the spectrum analyzer. (b) The scanning electron microscope picture of central part of the device (rotated by 90^0 with respect to the upper figure).

structures were made of Au (300 nm thick) by means of optical lithography on a lightly doped silicon wafer with a 500 nm thermal oxide surface layer. The rest of the structure, the Py strip (25 nm thick) with 0.3×3 μm^2 lateral size and the Cu leads (80 nm thick), were made using electron-beam lithography and lift-off. The left and right CSW are designed to have nearly 50 Ω impedance [24] and connected by means of microwave picoprobes to an rf signal generator (SG) and a spectrum analyzer (SA) respectively. For all measurements the output power of the signal generator was set at 20 dBm (100 mW), however the power that reaches the sample is significantly reduced.

As shown in Fig.3.1(a), when an alternating current flows through the shorted-end of a CSW, it generates an rf, transverse to the strip, magnetic field $h_{rf}(t)$. This field creates a flux (the primary flux) through the Py/Cu loop and induces voltage in the loop according to Faraday's law. Furthermore, if the frequency of the rf field is equal to the frequency of magnetization precession of the Py strip (i.e FMR condition), the resonant magnetization precession creates an additional flux (the FMR flux) through the loop, as well as additional induced voltage. Thus the measured signal corresponds to a superposition of primary and FMR fluxes.

Measurements are done by sweeping a dc magnetic field H_0 applied along the Py strip and perpendicular to h_{rf}, while the generated voltage at the applied rf field frequency was measured by a spectrum analyzer. In order to increase the signal-to-noise ratio a frequency locked technique in a 10Hz spectral bandwidth was employed. All the measurements are done at room temperature.

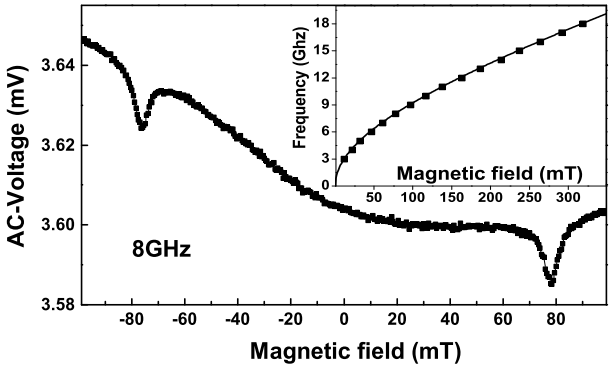

Figure 3.2: The measured *ac* voltage as a function of *dc* magnetic field for an applied transverse rf magnetic field frequency $8GHz$. The inset shows the *dc* magnetic field dependence of the resonant frequency corresponding to the dip in the measured voltage vs. magnetic field. The squares represent the experimental data points, while the curve is the fit to the data using Kittel's equation.

3.3 Results and discussion

Fig.3.2 shows a typical output signal as a function of the dc magnetic field (H_0), taken for an rf field frequency of 8 GHz. Two well defined 20 μV dips at $H_0 = \pm 80\ mT$ are observed on top of a few mV background. By measuring the transmitted power on a chip without the ferromagnetic strip, it was found that the background signal is unrelated to FMR and can be further omitted from consideration.

The inset to Fig.3.2 shows the position of the dip for different frequencies of the rf field as a function of the applied *dc* field. The squares correspond to the experimental data, while the solid line is the fit with Kittel's equation for the uniform precession mode [20]: $\omega_0^2 = \gamma^2 H_0 (H_0 + M_S)$, where $\gamma = g\mu_B\mu_0/\hbar$ is the gyromagnetic ratio which depends on the g factor and the Bohr magneton μ_B. From the fit, the saturation magnetization of the Py strip was found to be about $\mu_0 M_S = 1\ T$ and the gyromagnetic ratio γ=176 GHz/T. These values are consistent with earlier reports [26]. The excellent fit demonstrates that the magnetization vector of the Py strip was driven predominantly in the uniform precession mode by the rf field.

When the amplitude of the dip was measured as a function of intensity of the applied rf field, a linear dependence was found. Thus, the magnetization precession around the direction of an effective field, results in a small time-dependent component of magnetization perpendicular to the easy axis $\vec{M}(t) = m_x(t) \cdot \hat{x} + m_y(t) \cdot \hat{y} + M_S \cdot \hat{z}$ and can be described by the linearized Landau Lifschitz Gilbert (LLG) equation [35]

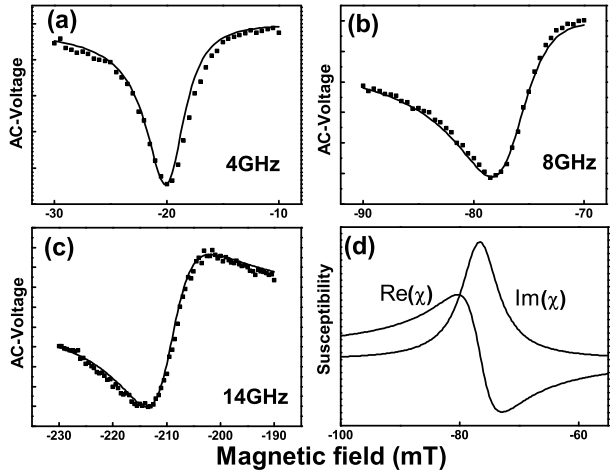

Figure 3.3: (a-c) The measured voltage across the sample as a function of the *dc* magnetic field, around the resonance position for three different frequencies $4GHz$, $8GHz$, $14GHz$, shown by squares. The line is the fit to the data using equation (3.3). (d) The *real* and the *imaginary* parts of the susceptibility $\chi(\omega)$ calculated using equation (3.2) for rf field frequency 8 GHz, $\gamma = 176\ GHz/T$, $M_S = 1\ T$ and $\alpha = 0.015$.

$$\frac{d\vec{M}}{dt} = -\gamma\vec{M} \times \vec{H}_{eff} + \frac{\alpha}{M_S}\vec{M} \times \frac{d\vec{M}}{dt} \tag{3.1}$$

where α is the dimensionless Gilbert damping parameter. We solved this equation under the assumption that the strip can be treated as a single domain thin film with a demagnetizing field only in the out-of-plane direction and the crystal anisotropy field is neglected, thus the effective field can be written as $\vec{H}_{eff} = [-m_y(t) + h(t)] \cdot \hat{y} + H_0 \cdot \hat{z}$.

The solution of this equation can be presented as the magnetic susceptibility tensor $\chi_{ij}(\omega)$. In our particular case only χ_{xy} and χ_{yy} components are required and since only the out-of-plane component of magnetization can create magnetic flux through the loop, the χ_{xy} can be excluded from consideration while the χ_{yy} has a form (further tensor indices are omitted for simplicity):

$$\chi(\omega) = \gamma M_S \frac{\gamma H_0 + i\omega\alpha}{\omega^2 - \omega_0^2 - i\omega\alpha\gamma(2H_0 + M_S)} \tag{3.2}$$

In Figure 3.3(d), we plot the real and imaginary parts of magnetic susceptibility as a function of the *dc* magnetic field (H_0) for an rf field of $8GHz$ frequency, with $\gamma = 176\ GHz/T$, $\mu_0 M_S = 1\ T$ and $\alpha = 0.015$. The imaginary part of $\chi(\omega)$ describes the out-of phase with respect ro driving

field magnetization precession. This results in the absorption peak observed in conventional FMR experiments, with a linewidth increasing linearly with frequency and being a function of α.

Figures 3.3(a-c) show the measured signal around the resonant frequency for three typical rf frequencies $4, 8$ and 14 GHz (the squares) from a different sample. We note here that the FMR dip shape changes from a Lorentzian to a more complex shape as frequency changes. This indicates a capacitive coupling between the left coplanar strips wave guide and the Py/Cu pick-up loop, meaning that, there is an extra contribution to the voltage created by the primary flux. This can also be understood as a phase shift (φ) between the voltage created by primary flux and the voltage due to the FMR flux. According to this, the change in voltage observed at resonance was fitted as a linear superposition of real and imaginary part of magnetic susceptibility:

$$\Delta V(\omega) = A(\omega) \cdot (Im[\chi(\omega)] \cdot cos(\varphi) + Re[\chi(\omega)]sin(\varphi)) \tag{3.3}$$

where $A(\omega)$ depends on the amplitude of the h_{rf} and on the coupling between the time dependent magnetization and the FMR flux generated by this. With $A(\omega)$ and φ as fit parameters, all the measured signals can be well fit. Figures 3.3 (a-c) show the fit results (solid lines) for three frequencies. This fit allows us to determine the Gilbert damping parameter, which was found to be $\alpha = 0.015$. This value is larger than the value $\alpha = 0.007$ commonly accepted for a thin film of Py [29, 36]. Our higher value may be due to magnetic inhomogeneities of the strip [37] and applied magnetic field and hardly due to the spin pumping[16] from the Py strip into the Cu contacts, as previously measured for a $Cu/Py/Cu$ structure[38, 13].

In summary, we demonstrate the detection of ferromagnetic resonance uniform mode of a single submicron ferromagnetic strip, embedded in an on-chip microwave transmission line device. We obtain the Gilbert damping parameter $\alpha = 0.015$. To our knowledge, samples used in this study are the smallest single structures (not spin valve or GMR type) in which the FMR have been measured by applying an ac magnetic field. We consider that the present experiment opens a new direction to study new mechanisms for controlling electron-spin accumulation in the lateral nanodevices at high frequencies.

Chapter 4

Detection of FMR assisted AMR effect

4.1 Aim of the experiment

Among the large variety of experimental techniques which are used for studying FM materials, such as SQUID magnetometry [39], magneto optical Kerr effect (MOKE) [40], Lorentz force microscopy [41] and magnetic force microscopy [42], *etc.*, the AMR technique (the anomalous magneto resistance effect) plays a rather important role since it is based on sensing electrical transport properties of FM.

It is an experimental fact that the resistance of a ferromagnet depends on relative orientation between current and magnetization. The phenomenological dependence is given as follows:

$$R(\theta) = R_0 + \Delta R cos^2\theta \tag{4.1}$$

where change in resistance $\Delta R/R_0$ is usually of the order of few percents and θ is an angle between current and magnetization.

Even though the mechanism of the AMR effect is not fully understood, the application of this technique shows a success in studying processes of magnetization reversal in ferromagnets [43].

The experiment which is presented in this chapter is designed to detect FMR by means of AMR measurement. We expect that if a *dc* magnetic field is applied along the ferromagnetic strip ($\vec{z}$ direction, Fig.4.1) then magnetization precession around $\vec{z}$ direction at the resonance will create an angle between current and magnetization resulting in change of the resistance of the FM strip.

From the magnitude of the AMR effect we expect to estimate cone angle of the precession, which is important for a spin-pumping experiment (see further Chapter 5), while typical parameters, which can be obtained in

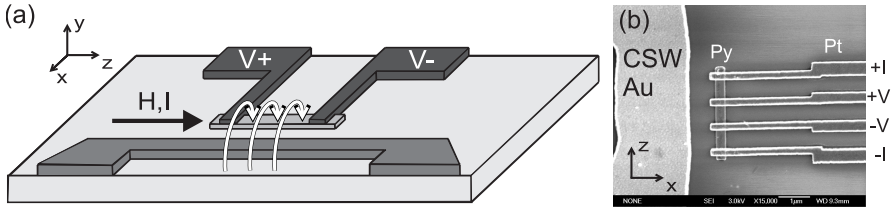

Figure 4.1: (a) Schematic picture of the device used in experiment. Rf magnetic field created by a Coplanar Strip Waveguide (CSW) drives a FMR resonance in a Py strip. By sending a dc current through the strip the voltage drop generated by FMR assisted AMR is measured between the platinum (Pt) contacts $V+$ and $V-$. (b) SEM picture of the central part of the device. External contacts are used for sending current, while voltage drop is measured between the inner contacts.

FMR experiment (saturation magnetization, Gilbert damping parameter, anisotropy fields) could be extracted from the shape of measured signal and dispersion law.

4.2 Device fabrication

The schematic diagram and SEM picture of device used in this experiment are shown in a Fig.4.1. Py strip is positioned at 2.5 μm distance from the microwave coplanar strip waveguide (CSW) and connected with the four platinum (Pt) leads which are used for sending current and detecting voltage drop across the strip (only two contacts are shown in a Fig.4.1(a)).

First the microwave strip waveguide structure was made on a Si/SiO_2 substrate by means of high current e-beam lithography followed by evaporation of 150 nm of gold (Au) layer on top of 10 nm adhesion titanium (Ti) layer.

At the second step, the Py structure was made using a low current e-beam lithography, followed by evaporation of 40 nm permalloy and further lift-off resulting in 3 μm long Py strip with a cross-section 40×300 nm^2.

The Pt leads have been made by means of low current e-beam lithography with a lift-off resulting in 80 nm thick Pt contacts.

In order to assure the clean contacts between Py and Pt leads, we use the Ar ion milling (Kaufmann etching) before the evaporation of platinum, which removes approximately 2 nm of Py. Platinum leads are evaporated right after etching without breaking the vacuum in evaporation chamber.

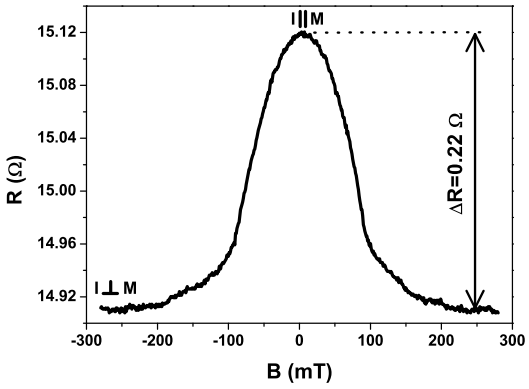

Figure 4.2: AMR signal for a Py strip. Magnetic field $\vec{B}$ is applied along the $\vec{x}$ direction (in plane of the strip but perpendicular to the $\vec{M}$).

4.3 Measurements and preliminary results

The AMR detection is done by means of four point contact resistance measurements as shown in Fig.4.1. This allows us to eliminate the voltage drop on the bonding wires.

A standard lock-in technique have been applied to measure a static AMR effect. Measured AMR curve for the magnetic field applied in-plane but perpendicular to $\vec{M}$ is shown in the Fig.4.2. Maximum modification of resistance, which corresponds to a 90 degrees θ angle was found to be $\Delta R = 0.22\ \Omega$ vs. $R_0 = 15.12\ \Omega$.

To measure the FMR assisted AMR effect (further AMR_{FMR}) we adopted a frequency modulation technique, where frequency of the rf-field was flipping between two values (f_{high} and f_{low}) separated by 5 GHz interval. The frequency of modulation was chosen to be the twice frequency of the lock-in resulting in the lock-in signal $V_{lock-in} = V_{low} - V_{high}$. This modulation allows to reduce the background dc offset which is originated mainly from the nonlinearities in a measurements setup, e.g. high frequency amplifier and so on.

During the measurements a dc magnetic field (B) is applied along the strip while frequencies of the driving rf field are shown as f_{high} and f_{low} horizontal lines in Fig.4.3(a).

For any value of the B other than the FMR condition, given by Kittel equation (Eq.2.10) we are expecting no voltage across the strip since the AMR response must be almost zero in this case (see vertical dashed lines B and D in Fig.4.3(a)).

When for one of the frequencies, either f_{high} or f_{low}, the FMR condition

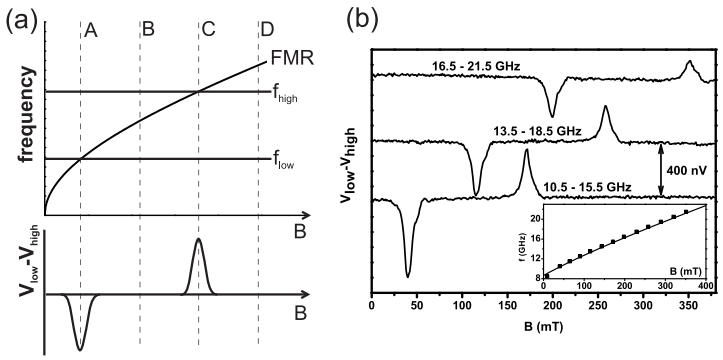

Figure 4.3: (a) Schematic illustration of the measurement scheme. Upper graph shows the FMR dispersion curve and two horizontal lines: f_{low} and f_{high}, which represents two frequencies of the modulated rf field. When one of the horizontal line crosses the dispersion curve the FMR assisted AMR signal is measured, where sign of the signal depends on either it corresponds to a resonance on a f_{low} or f_{high} - bottom half-plane. (b) Measured AMR_{FMR} signal for a lock-in modulated dc current $I = +400\ \mu A$ and three pairs of frequencies of modulated driving rf field with a frequency interval 5 GHz

is satisfied a voltage drop will occur along the strip due to the AMR_{FMR} effect.

During the experiment, a dc current is sent through the strip, while frequency modulation and lock-in voltage measurements were set to measure voltage as $V_{f_{low}} - V_{f_{high}}$. First resonance condition (at f_{low}) results in a negative measured voltage (dip at the vertical dashed line A) since resistance of the strip is smaller when magnetization and direction of the current are misaligned, i.e $V_{low} < V_{high}$. The second resonance (at f_{high}) leads to a positive voltage (peak at the vertical dashed line C), since now $V_{low} > V_{high}$.

Experimentally measured AMR_{FMR} curves are shown in the Fig.4.3(b) for different pairs of rf field frequencies, all at dc current $I = +400\ \mu A$.

Since the AMR_{FMR} signals, either peaks or dips, are expected only at FMR condition, we can find the FMR dispersion law. The inset on the Fig.4.3(b) shows the frequency of the FMR as a function of the applied dc magnetic field. Solid squares are experimentally measured points, while solid line is a fit with Kittel equation for a ferromagnetic strip magnetized along its easy axis $\vec{z}$:

$$\omega_0^2 = \gamma^2(H_0 + H_{an} + N_x M_s)(H_0 + H_{an} + N_y M_s) \tag{4.2}$$

where gyromagnetic ratio γ was taken to be 176 GHz/T, in plane demagnetizing factor $N_x = 0.1$, out-of plane demagnetizing factor $N_y = 0.9$

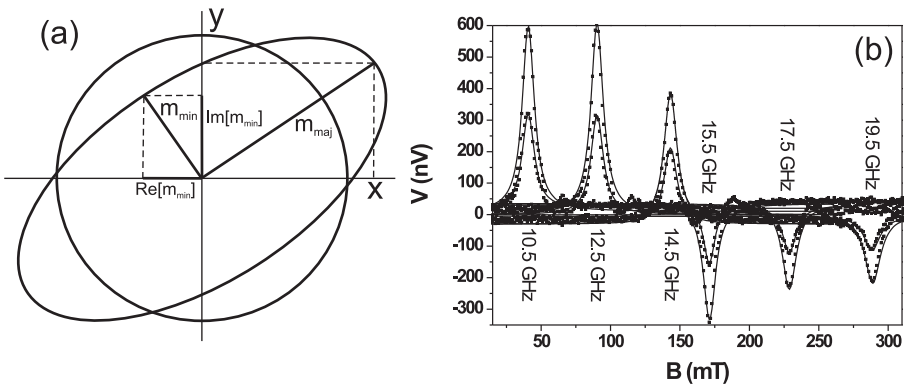

Figure 4.4: (a) Sketch of transformation from elliptical trajectory to the circular one for a slightly off-resonance condition: tilted ellipse is a real trajectory, circle is a mean circular trajectory calculated as $m = (|m_{min}| + |m_{maj}|)/2$. (b) Shapes of the AMR_{FMR} signals as a function of *dc* magnetic field for a different frequencies of driving field and two currents $I = -200,\ -400\ \mu A$. Dots are experimental points. Solid lines are fit with expression (4.4)

and $H_{an} = 5\ mT$, which is originated from remanent magnetization of our magnet.

In order to find how the shape of the measured signals evolves when magnetic field is swept through the resonance, we treat our system as an elliptical precession of the magnetization.

Since the FMR frequency is much larger than our data acquisition rate (lock-in frequency is 17 Hz and lock-in time constant is 1 *sec*, while FMR is in a range of GHz frequencies) we assumed that AMR_{FMR} signal will be sensitive to the mean θ angle over the one precession period. Therefore, θ angle in equation (4.1) was taken to be $\theta = (\theta_x + \theta_y)/2$.

Angle θ as a function of frequency of driving field and applied magnetic field can be written via the high frequency magnetic susceptibility functions (Sec.2.5 of this thesis):

$$\theta(\omega, B) = \frac{h_0}{2M_s}(|\chi_L(\omega, B)| + |\chi_T(\omega, B|) \tag{4.3}$$

where h_0 is an amplitude of the driving rf field, M_s is a saturation magnetization of the Py strip and χ_L and χ_T are magnetic susceptibility functions.

We take modulus of the χ since at off-resonance condition, the major and

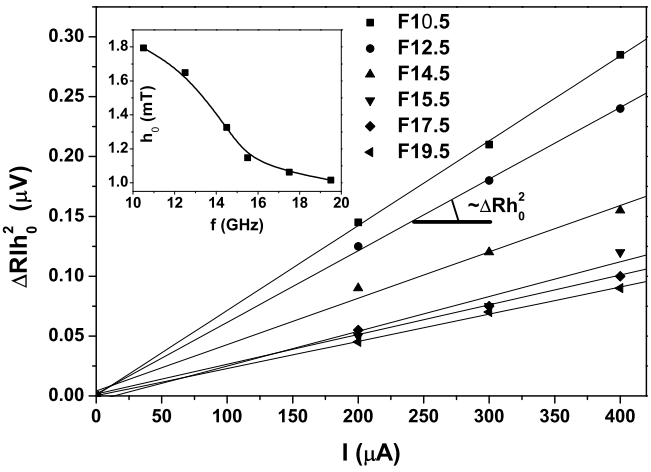

Figure 4.5: Fitting AMR_{FMR} amplitude (ΔRIh_0^2) as a function of *dc* current (I) for different frequencies of rf field. Inset: Amplitude of the rf field induced by CSW as a function of frequency calculated from the slope of the $\Delta RIh_0^2(I)$ lines with $\Delta R = 0.22\ \Omega$.

minor axes of ellipse drawn by the vector of magnetization do not coincide with x and y axes, as shown at fig.4.4(a).

Using phenomenological expression for the AMR effect (Eq.4.1), under the small angle approximation with θ angle dependence on the frequency and the magnetic field (4.3) we fit shape of the measured signal for few typical frequencies and *dc* currents values (Fig.4.4) using the Gilbert damping parameter α and the amplitude of the rf field as a fitting parameters. The fitting expression therefore takes a form:

$$V_{AMR} = \Delta RI\theta^2(h_0, \alpha) \tag{4.4}$$

where $\Delta R = 0.22\ \Omega$ is a maximum of the AMR_{FMR} effect which would be observed for a 90 degrees θ angle and I is a *dc* current sent through the strip.

On a basis of the fitting procedure we found that Gilbert damping parameter α is decreasing from 0.012 to 0.009 as the frequency of driving field increases.

Plot of the value ΔRIh_0^2 as a function of applied *dc* current (Fig.4.5) allows us to find the frequency dependence of the rf field amplitude induced by CSW. Function $h_0(f)$ is shown in the inset of Fig.4.5 and was calculated from the lines slope, which gives ΔRh_0^2.

Since the found Gilbert damping parameter is larger than that for bulk Py ($\alpha = 0.007$) we can think about number of FMR line broadening mechanisms such as nonuniform magnetization dynamics and spin-pumping effects.

Effects of the nonuniform magnetization dynamics which account for the inhomogeneity of the magnetic field and the sample predict line width narrowing with increasing frequency, since for large excitation frequencies, the dispersion curves for uniform precession and spin wave excitations are coming closer to each other (Fig.6.3, Chapter 6 of this thesis.)

Effects of the spin pumping (angular momentum loss via the spin transport to an adjacent normal metal) at first glance should lead to the resonance line broadening [13]. However, as will be shown in the Chapter 5, the loss of angular momentum depends on the cone angle of the precession. Therefore we assume that we are dealing with an interplay between increasing of momentum loss and decreasing of the delivered rf power to a system with increasing the frequency of the rf field (inset Fig.4.5).

In summary, we demonstrated the detection of the uniform resonance precession mode of magnetization of a small ferromagnetic strip using the effect of FMR assisted AMR. Dispersion law of the measured FMR is in good agreement with the one predicted by Kittel (Eq.2.10), while analysis of the shape of the resonance signal allows us to estimate the amplitude of the rf magnetic field, which is created by a coplanar strip waveguide.

Measured effect of narrowing line width with increasing frequency of the rf field requires more detailed analysis of both the mechanism of FMR assisted AMR and dynamics of magnetization precession, including nonlocal [14] and nonhomogeneous effects (Chapter 6).

Chapter 5

Charge battery operated by ferromagnetic resonance

5.1 Electronic transport through FM/NM interface

What makes a ferromagnetic metal to be different from a paramagnetic metal is the presence of a strong exchange interaction which aligns all the spins to orient in the same direction. This interaction will be mentioned in the frame of Heisenberg model (6.6), which can be generally called "localized model of ferromagnetism". However, when one starts to think about electronic transport properties of ferromagnetic metals, the model which is based on the localized spins is no longer useful. In contrast, spin dependent electronic transport can be described in the frame of Pauli-Stoner model of ferromagnetism, which essentially resembles the free electron model [20] but also takes into account the spin degree of freedom.

The principal idea of the Pauli-Stoner [44] model is that the conduction band can be split into two subbands, namely spin-up and spin-down (Fig.5.1). In paramagnetic metals these subbands are degenerate, which results in equal number of spin-up and spin-down electrons. However, in ferromagnets the exchange field releases this degeneracy, resulting in a shift of one subband with respect to another along the energy axis. Since the density of states at the Fermi level is different for the spin-up and spin-down subband, the number of conducting spin-up electrons will be larger than that for spin-down. At the same time, the difference in density of states for spin subbands also results in a different mobility for spin-up and spin-down electrons. On average this two effects are usually described by different spin-up and spin-down conductivity, which is known as "two current model" and was suggested by T.Valet and A.Fert [4].

The situation starts to be more complicated when transport is con-

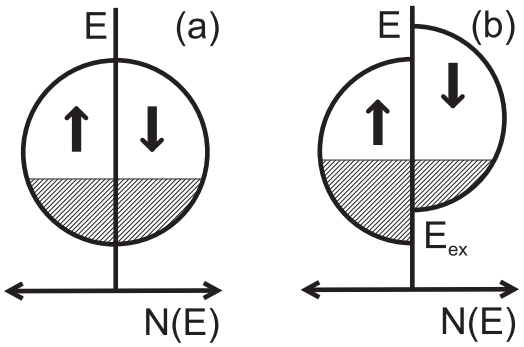

Figure 5.1: Schematic illustration of spin subbands for the conduction band of metals. (a) Paramagnetic metal: spin-up and spin-down subbands are degenerate; (b) Ferromagnetic metal: different concentration and different density of states for spin-up and spin-down electrons.

sidered through the NM/FM interface. One can imagine the situation when an electron enters the ferromagnet with spin polarization transverse to the magnetization of ferromagnet. This is be possible when current flows through $FM_1/NM/FM_2$ structure where magnetizations of two ferromagnets ($FM_{1,2}$) are not collinear. The transport through this type of interfaces is described by the matrix of interface conductance where the diagonal elements are spin-up and spin-down interface conductances, while the off-diagonal elements are the so-called spin mixing conductances $g^{\uparrow\downarrow}$ and $g^{\downarrow\uparrow}$ which physically represent the probability of the transverse spin to flip either into spin-up or into spin-down state. A comprehensive analysis of spin mixing conductance in the frame of scattering matrix approach was made by Brataas *et. al.* [45] while the calculations using the band structure analysis were made by Xia *et. al.* [46]. Furthermore, since the mixing conductance is a property of interface between two materials, it also depends on their bulk properties [47].

5.2 Parametric spin pumping into NM driven by FMR

It was shown by Hernando *et. al* [48] that if the magnetization of FM follows the resonant precessional dynamics this leads to the modulation of interface conductance. Later Tserkovnyak *et. al.* [16] have shown that this conductance modulation leads to the spin current flow into the NM, or in easy words to the "spin pumping".

The spin pump current is governed only by the spin mixing conductance and the dynamics of the FM magnetization:

$$\vec{I}_s^{(p)} = \frac{\hbar g^{\uparrow\downarrow}}{4\pi}\vec{m} \times \frac{d\vec{m}}{dt} \tag{5.1}$$

One can easily find some similarities of this expression with Gilbert damping term in LLG equation (2.4), which is a signature of the fact that spin pumping can be considered as an additional channel for damping of precessional motion, as was indeed observed experimentally [49, 13].

When the spin current is pumped into the NM it builds up the spin accumulation $\vec{s}$ close to the FM/NM interface. In principle, the spin pumping current should have both *ac* and *dc* components. However, if the precession length ($l_\omega = \sqrt{D_N/2\pi\omega}$, where D_N is the electron diffusion coefficient in NM) is larger than the spin flip length, which is equivalent to $\omega\tau_{sf} < 1$ (τ_{sf} is a spin-flip time), then the *ac* component of spin current can be neglected since it will be averaged out by spin-flip processes.

In detail, vanishing of *ac* component is caused by absorption of the transverse spin current inside the ferromagnet on the scale of the so-called transverse spin-coherence length given by:

$$\lambda_{sc} = \pi/|k_F^{\uparrow} - k_F^{\downarrow}| \tag{5.2}$$

For transition metals Co, Fe, Ni and their alloys, λ_{sc} is at the order of Fermi wavelength thus is being an atomic length scale [50].

It is worthwhile to note that equation (5.1) gives spin current as a loss of angular momentum in FM, and since the units for angular momentum are the same as for $\hbar$, spin current is measured in the units of energy.

Usually it is convenient to talk about spin accumulation in terms of difference in spin chemical potentials. The spin accumulation in terms of angular momentum $\vec{s}$ can be converted into difference in spin chemical potential $\vec{\mu}_s^N$ using the density of states in NM:

$$\vec{\mu}_s^N = \frac{\vec{s}}{\hbar N(E_F)\Omega} \tag{5.3}$$

were $N(E_F)$ is an one spin density of states [1] at the Fermi level and Ω is the volume of NM.

Now, in order to rewrite the spin pumping equation (5.1) in terms of chemical potentials one must divide it by $\hbar N(E_F)\Omega$ from a both sides resulting in:

$$\vec{I}_s^{(p)} = \frac{d\vec{\mu}_s^N}{dt} = \frac{\hbar g^{\uparrow\downarrow}}{4\pi\tau_i}\vec{m} \times \frac{d\vec{m}}{dt} \tag{5.4}$$

[1] One spin density of states is twice smaller than electron density of states since the spin degeneracy is equal 2.

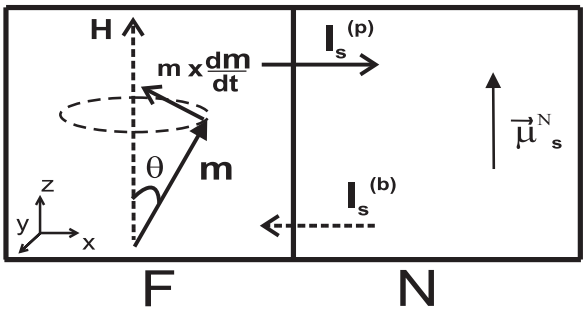

Figure 5.2: Schematic illustration of FM/NM interface. The ferromagnet due to the precessional dynamics pumps spin current into normal metal - $I_s^{(p)}$, this builds-up spin accumulation - μ_s^N, which induces back flow spin current into FM - $I_s^{(b)}$

.

where $\tau_i = \hbar N(E_F)\Omega$ plays the role of the spin injection time into the NM.

If one knows the dynamics of magnetization in a FM, then spin pump current can be easily calculated. If magnetization obeys resonant precessional dynamics then spin current can be expressed in terms of high frequency magnetic susceptibility $\chi(\omega)$:

$$I_s^{(p)} = -\frac{\hbar g^{\uparrow\downarrow}}{4\pi M_s^2} i\omega \chi_T(\omega)\, \chi_L^*(\omega)\, h_0^2 \tag{5.5}$$

where the result is given for precession in a thin ferromagnetic film (See Chapter 2).

Expression for the spin pumping can be also expressed in terms of the the resonance frequency and the precession cone angle:

$$I_s^{(p)} = \frac{\hbar\omega g^{\uparrow\downarrow}}{4\pi} \sin^2\theta \tag{5.6}$$

5.3 Spin battery operated by FMR

The pumping of the spin current is not the only process that occurs at the FM/NM interface. If there will be spin accumulation in NM it will lead to a back flow spin current into the FM. The balance between spin pump and spin back flow current will determine both the net spin current which flows through the interface and the steady state spin accumulation in a NM. This is known as a "spin battery" (Fig.5.2).

The spin battery problem was solved by Brataas *et. al.* [45], where in addition to the spin pump current, the back flow spin current and spin diffusion inside the NM were taken into account.

If the FMR frequency and the spin flip rate in both FM and NM are smaller than typical spin escape rate (rate of spin injection through the FM/NM interface τ_i^{-1}), then it leads to the situation when electrons can go back and forth through the FM/NM interface without changing their spin state, resulting in cancellation of the component of the spin current parallel to the instantaneous magnetization direction $\vec{m}$ by spin back flow.

Under the above condition the non zero back flow spin current is defined only by transversal to $\vec{m}$ component of the spin accumulation:

$$\vec{I}_s^{(b)} = -\frac{g^{\uparrow\downarrow}}{4\pi\tau_i^2}\vec{m} \times (\vec{s} \times \vec{m}) \tag{5.7}$$

The relation between the spin accumulation μ_s^N and spin current $I_s = I_s^{(p)} + I_s^{(b)}$ is governed by the spin-diffusion equation:

$$\frac{\partial\vec{\mu_s}}{\partial t} = D_N\frac{\partial^2\vec{\mu_s}}{\partial x^2} - \frac{\vec{\mu_s}}{\tau_{sf}} \tag{5.8}$$

where the second term accounts for spin relaxation where τ_{sf} is a spin flip time and D_N is a diffusion coefficient in a NM.

Diffusion equation must be solved with the boundary condition given by the spin current continuity equation at the interface ($x = 0$):

$$\frac{D_N}{\Omega}\frac{\partial\vec{\mu_s}}{\partial x} = -\frac{\vec{I_s}}{A} \tag{5.9}$$

where A is a cross section of the FM/NM interface.

The spin diffusion equation gives the steady state spin accumulation in terms of the net spin current through the FM/NM interface:

$$\mu_s(x) = \frac{I_s\lambda_{sf}\Omega}{AD_N}exp(-x/\lambda_{sf}) \tag{5.10}$$

where $\lambda_{sf} = \sqrt{D_N\tau_{sf}}$

If we assume circular magnetization precession, then the spin pump equations (5.4) and equation for the spin back flow (5.7) together with the solution for the diffusion equation (5.10) lead to an expression for the spin accumulation in NM close to the interface ($x \to 0$):

$$\mu_s^N = \hbar\omega_0\frac{\sin^2\theta}{\sin^2\theta + \eta} \tag{5.11}$$

where θ is a cone angle of magnetization precession while η is a reduction factor given by:

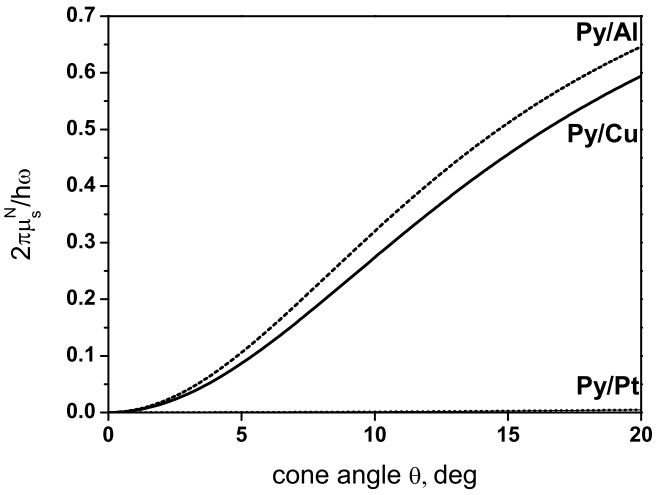

Figure 5.3: Spin accumulation (in units of $\hbar\omega$) as a function of precession cone angle for Py/Cu (solid line) and Py/Al (dashed line) interfaces at room temperature. The simulation is made in a frame of Brataas *et. al.* "spin battery" model [45]. The dashed line along the horizontal axis corresponds to negligible spin accumulation at Py/Pt interface.

$$\eta = \frac{4\pi A N(E_F)\hbar}{g^{\uparrow\downarrow}} \sqrt{\frac{D}{\tau_{sf}}} \tag{5.12}$$

which shows the ratio between spin injection time and effective spin dissipation time which accounts for both spin-flip and spin diffusion processes.

For Py/Cu interface: mixing conductance in the units of number of conducting channels per area is $g^{\uparrow\downarrow}/A = 1.5 \times 10^{15}\ cm^{-2}$ [51], spin diffusion length for Cu at room temperature is $\lambda_{sf} = 350\ nm$ [2] while spin flip time is $\tau_{sf} = 42\ ps$ [6], one-spin density of states is $N(E_F) = 1.74 \times 10^{28}\ eV^{-1}\ m^{-3}$ [51] and $\hbar = 6.58 \times 10^{-16}\ eV \cdot s$. This results in $\eta = 0.08$.

For Py/Al interface: mixing conductance in the units of number of conducting channels per area is $g^{\uparrow\downarrow}/A = 1.5 \times 10^{15}\ cm^{-2}$ [3], spin diffusion length for Al at room temperature is $\lambda_{sf} = 600\ nm$ while spin flip time is $\tau_{sf} = 124\ ps$ [6], one-spin density of states is $N(E_F) = 2.4 \times 10^{28}\ eV^{-1}\ m^{-3}$ [51]. This results in $\eta = 0.064$.

[2] It appears more easy to find in literature the spin flip length rather then diffusion coefficient. Therefore we have used relation $\lambda_{sf} = \sqrt{D\tau_{sf}}$.

[3] No literature number was found, so assumed to be the same as for Cu.

For Py/Pt interface: mixing conductance in units of number of conducting channels per area is $g^{\uparrow\downarrow}/A = 1.76 \times 10^{15}\ cm^{-2}$ [51], spin diffusion length for Pt at room temperature is about $\lambda_{sf} = 5\ nm$ while spin flip time is $\tau_{sf} = 10\ fs$ and one-spin density of states is $N(E_F) = 1.04 \times 10^{29}\ eV^{-1}\ m^{-3}$ [51]. This results in $\eta = 24.4$.

The spin accumulation as a function of precession cone angle (Eq.5.11) is plotted for Py/Cu, Py/Al and Py/Pt interfaces in Fig.(5.3).

Almost negligible spin accumulation in the Pt is a result of the high rate of spin flip processes which makes the Pt an almost perfect "spin sink". Namely, every injected into the Pt spin will flip its state very fast (e.g. faster then frequency of the magnetization precession), which can be observed in FMR experiment as a FMR line broadening caused by the angular momentum loss.

5.4 Charge battery operated by FMR

The spin battery treatment only focuses on the spin transport. However, spin transport is always accompanied with a charge transport since spins are carried by electrons. Therefore these two processes must be considered self-consistently.

When a spin current is flowing through the interface, it can be seen as two electrons with different spin polarization, where one is entering FM while another one is leaving. At a first glance this should result in a zero net charge current. However, in a FM, conductivities for spin-up and spin-down electrons are different, which means that processes of entering and leaving FM occur at different rates resulting in charge accumulation close to the FM/NM interface.

The equation for charge current through the FM/NM interface in general case can be written as:

$$I_c = \frac{eg}{h}\left[\left(\mu_0^F - \mu_0^N\right) + 2p(\vec{m}\cdot\vec{\mu}_s^F) - 2p\left(\vec{m}\cdot\vec{\mu}_s^N\right)\right] \tag{5.13}$$

where $\mu_0^F - \mu_0^N$ is the difference in electrochemical potential at the interface due to the charge accumulation, $\vec{\mu}_s^F$ is the spin accumulation in the FM and $\vec{\mu}_s^N$ is the spin accumulation in NM, $\vec{m}$ is a unit vector of instantaneous direction of magnetization in FM, $g = (g^\uparrow + g^\downarrow)/2$ is the two channel conductance and $p = (g^\uparrow - g^\downarrow)/(g^\uparrow + g^\downarrow)$ is the interface spin polarization.

When there is no bias voltage applied across the interface the steady state charge current should vanish which allows us to write the built-in interface voltage as a function of spin accumulation close to the interface:

$$\frac{\mu_0^F - \mu_0^N}{e} = \frac{2p}{e}\left[(\vec{m}\cdot\vec{\mu}_s^N) - (\vec{m}\cdot\vec{\mu}_s^F)\right] \tag{5.14}$$

If we assume strong spin relaxation processes in a ferromagnet and high spin injection rate into NM, then one can neglect spin accumulation in FM ($\mu_s^F = 0$) and take Brataas solution [45] for spin battery (μ_s^N spin accumulation in NM) resulting in a voltage across the FM/NM interface given by:

$$V = \frac{2p}{e}\mu_s^N = \frac{2p}{e}\hbar\omega_0\frac{\sin^2\theta}{\sin^2\theta + \eta} \tag{5.15}$$

Thus, for frequency $10^{11}\ Hz$, cone angle of precession $\theta \simeq 10\ deg$ and typical spin polarization for Py/Cu interface $p = 0.4$ [52], the expected voltage across the interface is $V \simeq 1\ \mu V$.

It is important to note that the above result is obtained under the assumption that spin injection time (τ_i) is much smaller than both spin flip time (τ_{sf}) and elastic electron scattering time(spin diffusion away from FM/NM interface). Under this approximation, electrons can go back and forth through the interface without flipping their spin state resulting in the cancellation of the back flow spin current with polarization collinear with $\vec{m}$. However, this assumption is quite counterintuitive since in order to have back and forth movement in diffusive systems, a large rate of elastic scattering processes is necessary which will increase spin diffusion into the bulk.

The comprehensive model of the charge battery driven by FMR is made by Xuhui Wang *et. al.* [17]. In that model the authors accounted for: i)spin emission (pumping) from FM into NM due to the precession of magnetization, ii) spin back flow due to the spin accumulation in NM, where the parallel to $\vec{m}$ component is not neglected, iii) spin diffusion in both FM and NM region. The set of diffusion equations is solved self-consistently with boundary conditions given by conservation of the net spin and charge currents through the FM/NM interface. The final result is given in terms of voltage across the interface as a function of the precession cone angle, frequency of the FMR and spin diffusion length both in NM and in FM.

Under the above conditions the back flow spin current equation takes a form:

$$\vec{I}_s^{(b)} = \frac{g}{4\pi\tau_i}\left[p\left(\mu_0^F - \mu_0^N\right) + \vec{m}\cdot\vec{\mu}_s^F - \vec{m}\cdot\vec{\mu}_s^N\right]\vec{m} - \frac{g^{\uparrow\downarrow}}{4\pi\tau_i}\vec{m}\times\vec{\mu}_s^N\times\vec{m} \tag{5.16}$$

where $g = (g^\uparrow + g^\downarrow)/2$ is a two channel conductance and $p = (g^\uparrow - g^\downarrow)/(g^\uparrow + g^\downarrow)$ is an interface spin polarization.

The difference between this equation and back flow spin current equation used by Brataas (5.7) is the first term that accounts for the spin current biased by built-in interface voltage and parallel to $\vec{m}$ spin accumulation in FM and in NM.

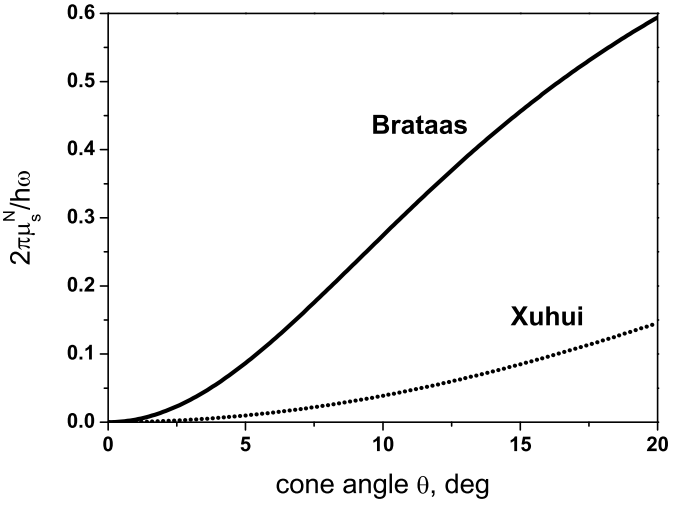

Figure 5.4: Spin accumulation (in units of $\hbar\omega$) as a function of precession cone angle for Py/Cu interface. Solid line - Brataas "spin battery" model [45], Dashed line - Xuhui Wang's model [17].

Using equation (5.14) the voltage drop across the interface $(\mu_0^F - \mu_0^N)/e$ can be excluded, which allows us to write back flow spin current only as a function of spin accumulation in NM and FM. Later, by neglecting spin accumulation in FM ($\vec{\mu}_s^F = 0$) and the terms proportional to p^2, the net spin current through the interface takes form:

$$\vec{I}_s = \frac{\hbar g^{\uparrow\downarrow}}{4\pi\tau_i}\vec{m} \times \frac{d\vec{m}}{dt} - \frac{g}{4\pi\tau_i}\left(\vec{m} \cdot \vec{\mu}_s^N\right)\vec{m} - \frac{g^{\uparrow\downarrow}}{4\pi\tau_i}\vec{m} \times \vec{\mu}_s^N \times \vec{m} \qquad (5.17)$$

where the first term is a spin pumping from FM into NM, while the second and the third are back flow of parallel and perpendicular to $\vec{m}$ spin current respectively.

Together with the result (5.10) one finds the spin accumulation in NM close to the interface:

$$\mu_s^N = \frac{\hbar\omega \sin^2\theta}{\sin^2\theta + (g/g^{\uparrow\downarrow})\cos^2\theta + \eta} \qquad (5.18)$$

A comparison between the Brataas model [45] and the Xuhui Wang's model [17] is shown in Fig.(5.4) for Py/Cu interface with two-channel conductance being $g = 1.03 \times 10^{15}\ cm^{-2}$ [51].

Xuhui model shows s significantly reduced spin accumulation since it also accounts for spin back flow current parallel to $\vec{m}$.

In summary, it is useful to point out that the phenomenon of spin transport through the FM/NM interface induced by the magnetization dynamics in FM cannot be described by the simple model since it must self consistently include the dynamics of magnetization in FM, spin dynamics in NM, spin and charge transport through the FM/NM interface.

In the presented in this chapter model, we assumed that the spin transport impact on the magnetization dynamics can be accounted as an increase in the effective Gilbert damping parameter, while the treatment of spin and charge transport through the interface can be done separately, which allows us to calculate spin accumulation in NM. The voltage drop across the interface has been calculated as $V = p\mu_s^N$ (when spin accumulation in FM is neglected), where p is a spin polarization of the interface.

Accounting of the spin accumulation in FM will lead to the smaller spin accumulation in NM and will require the renormalization of the interface spin polarization in order to account for that transport which will take part in the bulk part of FM.

Chapter 6

Nonuniform dynamics of magnetization

6.1 Magnetization dynamics: energy consideration.

All the considerations of magnetization dynamics presented in the previous sections were based on the torque equation (2.1) or, in case of damping, on the LLG equation (2.3), where the magnitude of magnetization $\vec{M}$ was taken to be unchanged.

However, the effective magnetic field - $\vec{H}_{eff}$, in principle, depends on magnetization itself. In case of uniformly magnetized film this dependence comes from demagnetizing field. In case of nonuniform magnetization few more effects must be taken into account. In order to do that it is convenient to write the equation of motion in terms of free energy of the ferromagnet [15] using Hamiltonian formalism of generalized coordinates and momentum [53]:

$$\frac{d\vec{M}}{dt} = \gamma\vec{M} \times \frac{\partial U_{free}}{\partial \vec{M}} + \frac{\alpha}{M_s}\vec{M} \times \frac{d\vec{M}}{dt} \tag{6.1}$$

where U_{free} is magnetic free energy, which depends on the magnetization itself. The derivative $-\partial U_{free}/\partial \vec{M}$ results in an effective magnetic field by analogy with mechanical gradient of the energy over coordinates, which results in force.

It is easy to see that equation (6.1) resembles the LLG equation with only the difference that magnetic field is replaced by its expression in terms of the free energy. This is indeed an important achievement, since energy of the ferromagnetic can be easily corrected by introducing new terms, if necessary.

As an example, lets write an energy of the ferromagnetic thin film:

$$U_{free} = U_{ex} + U_{mag} + U_a \tag{6.2}$$

where U_{ex} is an exchange energy, which is assumed to be uniform, U_a is a crystalline anisotropy energy, which in case of polycrystalline permalloy can be neglected and U_{mag} is a magnetic energy, which can be written as:

$$U_{mag} = U_Z + U_M \tag{6.3}$$

where $U_Z = -\vec{M}\vec{H}_0$ is the Zeeman energy of the magnetization interaction with an external magnetic field and U_M is the demagnetization energy which is originated from dipole-dipole interaction and depends on the shape of the ferromagnet. In case of the tangentially magnetized thin film, demagnetization energy takes the form:

$$U_M = N_{ij} M_i M_j \tag{6.4}$$

Derivation of U_{free} over the $\vec{M}$ leads to the following expression for the effective field:

$$H_i^{eff} = H_i^0 - N_{ij} M_j \tag{6.5}$$

which is the same as was assumed in section (2.3). In the rest of this chapter it will be shown that energy consideration allows to account for nonuiniform precession of magnetization.

6.2 Energy and effective exchange field of the nonuniformly magnetized ferromagnet

The uniform precession of vector of magnetization results from precession of all the magnetic dipole moments (*e.g.* spins) which constitute macro-spin. As was suggested by Heisenberg, an energy of exchange interaction between two spins can be written as:

$$U_{ex} = -J\vec{M}_1\vec{M}_2 \tag{6.6}$$

where J is the exchange integral, while $\vec{M}_i$ are magnetic moments of the neighboring spins.

As follows from the Heizenberg equation (6.6), uniform precession of the magnetization results in uniform exchange energy in a sample, that is why it has no contribution to the effective field Eq.(6.5).

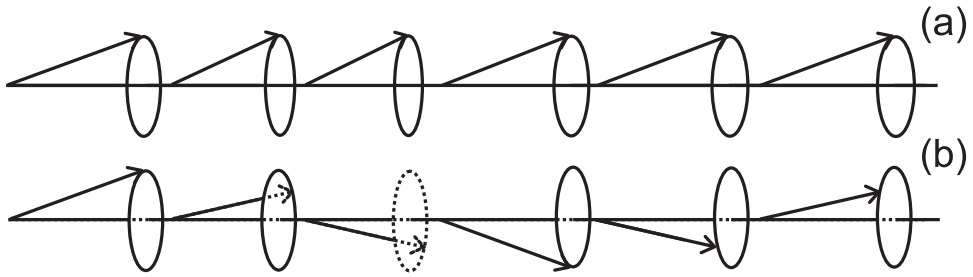

Figure 6.1: Schematic representation of different magnetization precession modes.(a)Uniform precession mode: all the spins are precessing in-phase; (b) Non-uniform precession mode: constant phase shift between two neighboring spins (spin wave mode).

However, if exchange energy is not homogeneous, it can be written as a sum of uniform energy U_0 and nonuniform part U_q, which represents increasing in exchange energy due to nonparallel orientation of the neighboring magnetic moments. The uniform part is given by equation (6.6), while U_q can be written as:

$$U_q = \frac{1}{2}\sum_{p=1}^{3}\sum_{s=1}^{3} A_{ps}\frac{\partial \vec{M}}{\partial x_p}\frac{\partial \vec{M}}{\partial x_s} \tag{6.7}$$

where one can easily recognize the quadratic term in a vectorial Taylor expansion of the exchange energy in the vicinity of its minima with A_{ps} being the tensor of the expansion coefficients. In an isotropic ferromagnet, which is the case, when a crystal anisotropy field can be neglected, A_{ps} is a scalar, and the effective field of the exchange interaction can be found easily just by differentiating equation (6.7) over $\vec{M}$ resulting in:

$$\vec{H}_q = A\nabla^2\vec{M} \tag{6.8}$$

When magnetization $\vec{M}$ can be written as a sum of constant $\vec{M}_s$ and spatially-dependent component $\vec{m}(\vec{r})$, the effective exchange field will have only spatial-dependent component. If the spatial dependence of $\vec{m}$ has a wavelike form, then the effective field starts to read as:

$$\vec{h}_q = -Dq^2\vec{m} \tag{6.9}$$

where $D = A/M_s$ and is known as the spin stiffness constant, while q is a wave vector.

6.3 Magnetic dipole-dipole interaction in a nonuniformly magnetized ferromagnet

As was mentioned before, the demagnetizing field has a dipolar nature. Thus, in the out-of-plane magnetized thin film, demagnetizing field can be found from Maxwell's equation:

$$\vec{B} = \mu_0(\vec{H} + \vec{M}) \tag{6.10}$$

Further continuity of magnetic induction $\vec{B}$ at the interface requires magnetic field $\vec{H}$ inside FM to be equal to $-\vec{M}\vec{n}$ since the magnetization outside the film is equal to zero. Therefore, for uniformly magnetized film demagnetizing field equals $\vec{H}_d = -\vec{M}\vec{n}$, where $\vec{n}$ is a unit vector perpendicular to the surface of the film. From similar consideration we can arrive at the uniaxial magnetization of the FM strip.

The physical origin of the demagnetizing field is a dipole-dipole interaction of non-compensated magnetic dipoles at the surface of the magnetic sample (surface magnetic charges [54]).

If a ferromagnetic film is non-uniformly magnetized, then it will result in spatial distribution of surface magnetic charges and dipole-dipole interaction must be calculated from the first principle using the following expression:

$$U_{dd} = -\frac{1}{2}\int_{\Omega} d^3x\psi\left(\vec{x}\right)\rho_m\left(\vec{x}\right) \tag{6.11}$$

where Ω is a volume of FM film, $\psi(\vec{x})$ is a magnetic potential which must be found from Poison equation $\Delta\psi(\vec{x}) = -\rho_m(\vec{x})$, with $\rho_m(\vec{x})$ being the magnetic charge density which is given by $\rho_m(\vec{x}) = -\nabla\vec{M}(\vec{x})$.

Equation (6.11) can not be solved in general case, however, for a thin film with inhomogeneity described by the wave vector $\vec{q}$ lying in the plane of the film approximate solution was derived by Herring and Kittel [55]:

$$H_d = -(\vec{M}\vec{n})sin^2\theta_q \tag{6.12}$$

where θ_q is the angle between the direction of the wave vector and the magnetization (Fig.6.2).

Similar expression was obtained by Kalinikos and Slavin for a long wave magnetic charge modulation in a film of finite size [56]:

$$H_d = -(\vec{M}\vec{n})F_{pp}(qd) \tag{6.13}$$

where F_{pp} is the matrix element of the magnetic dipole interaction which can be found in related reference, d is a thickness of the film, while $p = 0, 1, 2, \ldots$ is a quantization number of magnetization waves for the out of plane component of wave vector $\vec{q}$.

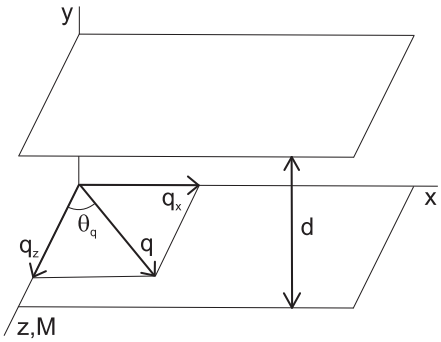

Figure 6.2: Sketch of magnetization wave excitation in a thin ferromagnetic film of thickness d. Wave vector of excitation lies in plane of the film and has arbitrary angle with respect to direction of saturation magnetization defined as θ_q.

6.4 Spin wave resonance

Since FMR experiments have been started, in addition to the uniform precession mode, higher energy modes have been observed [57]. These new modes have been assigned to the spin-wave excitations (SW).

Dispersion relations for the spin waves can be derived using the analysis of the nonhomogeneous magnetization presented in the previous section. Thus, the LLG equation (2.3) must be solved with accounting for an exchange field and modified dipole-dipole interaction, however it is easy to see that without losing generality, a solution can be obtained by simply replacing H_0 with $H_0 + Dq^2$ and accounting for correction in demagnetizing field resulting in:

$$\omega_{SW}^2 = \gamma^2(H_0 + Dq^2)(H_0 + Dq^2 + M_s F_{pp}(qd)) \tag{6.14}$$

The obtained expression describes the resonance frequency of the spin wave excitation and different from the resonance frequency of the uniform precession mode given by Kittel equation (3.2), which is a signature of the contribution from the exchange and modified dipole-dipole interactions.

When $\vec{q}$ is large enough, the dipole-dipole interaction approaches zero while the exchange energy becomes larger than Zeeman energy $U_Z = -M_s H_0$ resulting in quadratic SW dispersion law $\omega = \gamma D q^2$ obtained in 1930 by Bloch [20].

More detailed analysis of the SW dispersion law (6.14) shows that two types of spin waves can be distinguished. When $\vec{q}$ is small, namely long wave excitation, the dipole-dipole interaction dominates over the exchange interaction resulting in the so-called dipole dominated surface wave (DDSW)

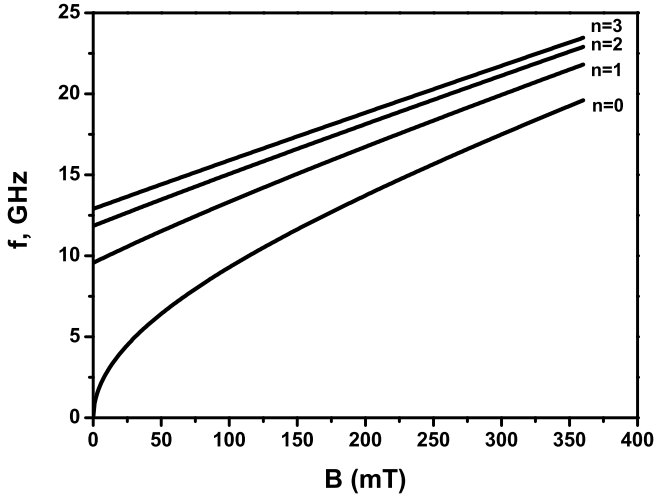

Figure 6.3: Dispersion low for the spin waves in Py film with thickness $d = 30\ nm$ and width $w = 300\ nm$. Wave vector is lying in a plane of the film but orthogonal to the $\vec{M}$. Frequencies of the $n = 0, 1, 2, 3$ modes as a function of magnetic field are shown.

mode or Damon-Eshbach (DE) mode [58]. In the opposite limit, when $\vec{q}$ is large, it leads to the exchange spin wave (ESW) mode.

If spin waves are excited in plane of the film with a $\vec{q}$ vector being perpendicular to $\vec{M}$ ($\vec{q} \perp \vec{M}$), then the exchange energy contribution can be neglected (long wave excitation) resulting in [59, 60]:

$$\omega_{SW}^2 = \gamma^2 \left[H_0(H_0 + M_s) + M_s^2 \frac{1 - e^{-2qd}}{4} \right] \tag{6.15}$$

When spin waves are spatially confined, as in a ferromagnetic strip, then the only allowed $\vec{q}$ vectors will be $n\pi/w$, where w is the width of the strip, while n is the spin wave quantization number, which is the number of nodes in a magnetization profile. It is easy to see that if $n = 0$, then it is corresponds to the uniform precession mode, which is a signature of the fact that uniform and nonuniform magnetization dynamics must be treated on the same basis.

The dispersion law calculated according to (6.15), for the spin waves ($\vec{q} \perp \vec{M}$) in Py film with thickness $d = 30\ nm$ and width $w = 300\ nm$ are shown in the Fig.6.3 for few quantization numbers n. For the larger n the effect of the exchange energy was taken into account since the requirement $qd \ll 1$ will not hold anymore.

Chapter 7

Conclusions

The aim of this project was an electrical detection study of the magnetization dynamics in Py/NM all metallic heterostructures in the presence of possible nonlocal spin dependent effects (e.g. spin pumping). The conclusions are summarized below:

- Theoretical studies of the uniform magnetization dynamics was made in the frame of the Landau-Lifshitz-Gilbert approach. Adopted for our experimental needs solutions for magnetization dynamics in tangentially magnetized thin ferromagnetic film and ferromagnetic strip have been obtained.

- Experimental detection of uniform magnetization precession in submicron Py strip has been done by means of magnetic flux pick-up method (RF detection). We have show the possibility of on-chip excitation and detection of FMR on submicron size scale.

- We performed an FMR assisted AMR experiment (the anomalous magnetoresistance) and demonstrated applicability of this technique for magnetization dynamics study (AMR detection). From the shape of measured signal we were able to estimate the amplitude of the rf magnetic field created by the coplanar strip waveguide used in the experiment.

- In both experiments on the FMR we observed an increase of Gilbert damping parameter α with respect to the value for bulk Py, which can be a signature of the nonuniform and nonlocal magnetization dynamics effects.

- Analysis of the existing spin pumping models has been made, which allows us to estimate the effect of the FMR driven charge battery at Py/Cu interface to be of order of 1 μV.

- A brief introduction into nonuniform magnetization dynamics is given. Dispersion law for the lowest dipole-dipole dominated spin wave modes are calculated in the frame of Damon-Eshbach approach.

Acknowledgements

Here I would like to say thanks to Marius Costache for a grate time we have spent together working on a subject which is the issue of this thesis. I really appreciate both the knowledge he shared with me and that freedom which I had during the last year. I owe the best words to Steve Watts for hours of discussing physics and hours of correcting grammatical mistakes in my notes (those mistakes which are still in this thesis were not corrected because of the hours we spent on borrel nights). I want to emphasize my gratitude to following people: Nikos Tombros for a lot of support with using EBL and clean-room facilities, Csaba Jozsa for reading carefully and giving brilliant comments on all the notes I gave him to read, soul and golden fingers of the group - Bernard Wolfs and Siemon Bakker for a lot of technical assistance in a lab and a lot of fun in a coffee room, Caspar van der Wal for his clear vision of physics and last but not least Bart van Wees for his motivating, even though sometimes hardly understandable, comments and guidelines. I had a nice time with FND group and happy that I stay here for my PhD study.

I say thanks to MSC/MCS^{plus} for giving me opportunity to study on 'Top Master Programm in Nanoscience' together with fantastic classmates: Cynne (Xinglan Liu), Anne Arkenbout, Abraham Slachter, Michiel Donker, Auke Kronemeijer and Ponky Ivo.

Maksym Sladkov, *Groningen, 12 July 2006.*

Bibliography

[1] M. N. Baibich, J. M. Broto, A. Fert, F. N. V. Dau, F. Petroff, P. Etienne, G. Creuzet, A. Friedrich, and J. Chazelas *Phys. Rev. Lett.*, vol. 61, p. 2472, 1988.

[2] I. Zutich, J. Fabian, and S. D. Sarma *Rev. Mod. Phys*, vol. 76, p. 323, 2004.

[3] N. F. Mott, Proc. R. Soc. London, Ser. A 153, 699 (1936), N. F. Mott, Proc. R. Soc. London, Ser. A 156, 368 (1936).

[4] A. F. T. Valet *Phys. Rev. B*, vol. 48, p. 7099, 1993.

[5] B. Dieny, V. S. Speriosu, S. S. P. Parkin, B. A. Gurney, D. R. Wilhoit, and D. Maur *Phys. Rev. B*, vol. 43, p. 1279, 1991.

[6] F. J. Jedema, A. T. Filip, and B. J. van Wees *Nature*, vol. 410, p. 345, 2001.

[7] L. Berger *Phys. Rev. B.*, vol. 54, p. 9353, 1996.

[8] J. C. Slonczewski *J. Magn. Magn. Mater.*, vol. 159, p. L1, 1996.

[9] M. Tsoi, A. G. M. Jansen, J. Bass, W. C. Chiang, M. Seck, V. Tsoi, and P. Wyder *Phys. Rev. Lett.*, vol. 80, p. 4281, 1988.

[10] E. B. Myers, D. C. Ralph, J. a Katine, R. N. Louie, and R. A. Buhrman *Science*, vol. 285, p. 867, 1999.

[11] A. Janossy and P. Monod *Phys. Rev. Lett.*, vol. 47, p. 612, 1976.

[12] R. H. Silsbee, A. Janossy, and P. Monod *Phys. Rev. B*, vol. 19, p. 4382, 1979.

[13] S. Mizukami, Y. Ando, T. Miyazaki, Phys. Rev. B. 66, 104413 (2002).

[14] Y. Tserkovnyak, A. Brataas, G. E. W. Bauer and B. I. Halperin, cond-mat/0409242.

[15] A. G. Gurevich and G. A. Melkov, *Magnetization Oscillations and Waves*. CRC Press, 1996.

[16] Y. Tserkovnyak, A. Brataas, and G. Bauer *Phys. Rev. Lett.*, vol. 88, p. 117601, 2002.

[17] Xuhui Wang, *in preparation*.

[18] L. D. Landau, E. M. Lifshitz, and L. P. Pitaevski, *Statistical physics, part*.2. Pergamon, Oxford, 3rd ed., 1980.

[19] T. L. Gilbert *Phys.Rev.*, vol. 100, p. 1243, 1955.

[20] C. Kittel, *Introduction to Solid State Physics*. John Wiley & Sons, 1996.

[21] C. P. Slichter, *Principles of magnetic resonance*. Springer, Berlin, 3rd ed., 1990.

[22] Thomas Gerrits, Coherent control of fast Precessional Dynamics in Magnetic Thin Films, PhD thesis, ISBN 90-9017662-4).

[23] R. C. LeCraw and C. S. P. E. G. Spencer *Phys.Rev.*, vol. 110, p. 1311, 1958.

[24] R. Garg, I. Bahl, P. Bhartia, and K. C. Gupta, *Microstrip Lines and Slotlines*. Artech House Publishers, 1996.

[25] S. Zhang, S. Oliver, N. Israelof, and C.Vittoria *Appl. Phys. Lett.*, vol. 70, p. 2756, 1997.

[26] F. Giesen, J. Podbielski, T. Korn, M. Steiner, A. van Staa, and D. Grundler *Appl. Phys. Lett.*, vol. 86, p. 112510, 2005.

[27] Z. Celinski, K. Urquhart, and B. Heinrich *J. Magn. Magn. Mater.*, vol. 166, p. 6, 1997.

[28] A. B. Kos, T. J. Silva, and P. Kabos *Rev. Sci. Inst*, vol. 73, p. 3563, 2002.

[29] T. J. Silva, C. S. Lee, T. M. Crawford, and C. T. Rogers *J. Appl. Phys.*, vol. 85, p. 7849, 1999.

[30] M. Schneider, T. Gerrits, A. Kos, and T. Silva *Appl. Phys. Lett.*, vol. 87, p. 072509, 2005.

[31] Y. S. Gui, S. Holland, N. Mecking, and C. M. Hu *Phys. Rev. Lett.*, vol. 95, p. 056807, 2005.

[32] J. Grollier, M. V. Costache, C. H. van der Wal and B. J. van Wees, accepted to J. Appl. Phys.

[33] Y. Acremann, C. H. Back, M. Blues, O. Portmann, A. Vaterlaus, D. Pescia, and H. Melchior *Science*, vol. 290, p. 492, 2000.

[34] C. Thirion, W. Wernsdorfer, and D. Mailly *Nature*, vol. 2, p. 524, 2003.

[35] T. L. Gilbert, Phys.Rev. **100**, 1243 (1955); L. D. Landau, E. M. Lifshitz and L. P. Pitaevski, Statistical physics, *part*.2, (Pergamon, Oxford, 3rd ed. 1980).

[36] T. Gerrits, T. J. Silva, J. P. Nibargera, and T. Rasing *J. Appl. Phys.*, vol. 96, p. 6023, 20054.

[37] B. K. Kuanr, R. E. Camley, and Z. Celinski *J. Magn. Magn. Mater.*, vol. 286, p. 276, 2005.

[38] S. Mizukami, Y. Ando, and T. Miyazaki *J. Magn. Magn. Mater*, vol. 226, p. 1640, 2001.

[39] W. Wernsdorfer, B. Doudin, K. Hasselbach, A. Benoit, J. Meyer, J. P. Ansermet, and B. Barbara *Phys. Rev. Lett*, vol. 77, p. 1873, 1996.

[40] A. O. Adeyeye, J. A. C. Bland, C. Daboo, J. Magn. Magn. Mat. 188. (1998), A. O. Adeyeye, J. A. C. Bland, C. Daboo, D. G. Husko, Phys. Rev. B 65, 3265, 1997.

[41] Y. Otani, S. G. Kim, K. Fukamichi, O. Kitachi, Y Shimada, 3M Intermag 98, Y. Otani, S. G. Kim, K. Fukamichi, O. Kitakami, Y Shimada, B. Pannetier, J. P. Nozieres, T. Matsuda, A. Tonomura, Proc. MRS Spring Meeting (San Francisco) 1997.

[42] R. O'barr, M. Lederman, S. Schultz, W. Xu, A. Scherer, and R. J. Tonucci

[43] Andrei Filip, Spin polarized electron transport in mesoscopic hybrid devices, PhD thesis , University of Groningen).

[44] S. Blundell, *Magnetism in Condensed Matter*. Oxford University Press, 2001.

[45] A. Brataas, Y. Tserkovnyak, G. E. W. Bauer, and B. Halperin *Phys. Rev. B*, vol. 66, p. 060404, 2002.

[46] K. Xia, P. J. Kelly, G. E. W. Bauer, A. Brataas, and I. Turek *Phys. Rev. B*, vol. 65, p. 220401, 2002.

[47] G. E. W. Bauer, Y. Tserkovnyak, D. Huertas-Hernando, and A. Brataas *Phys. Rev. B*, vol. 67, p. 094421, 2003.

[48] D. H. Hernando, Y. V. Nazarov, A. Brataas, and G. Bauer *Phys. Rev. B*, vol. 62, p. 5700, 2000.

[49] R. Urban, G. Woltersdorf, and B. Heinrich *Phys. Rev. Lett.*, vol. 87, p. 217204, 2001.

[50] M. D. Stiles and A. Zangwill *Phys. Rev. B.*, vol. 66, p. 014407, 2002.

[51] M. Zwierzycki, Y. Tserkovnyak, P. Kelly, A. Brataas, and G. E. W. Bauer *Phys. Rev. B.*, vol. 71, p. 064420, 2005.

[52] R. J. S. jr., J. M. Byers, M. S. Osofsky, B. Nadgorny, T. Ambrose, S. F. Cheng, P. R. Cheng, P. R. Broussard, C. T. Tanaka, J. Nowak, J. S. Moodera, A. Barry, and J. M. D. Coey *Science*, vol. 282, p. 85, 1998.

[53] L. D. Landau and E. M. Lifshitz, *Mechanics*. Pergamon, Oxford, 3rd ed., 1976.

[54] P. Lorrain and D. R. Corson, *Electromagnetic Fields and Waves*. W. H. Freeman and Company, 1972.

[55] C. Herring and C. Kittel *Phys. Rev.*, vol. 81, p. 869, 1951.

[56] B. A. Kalinikos and A. N. Slavin, J.Phys.C. 19, 7013 (1986).

[57] R. Weber and P. E. Tannenwald *Phys.Rev.*, p. A498, 1965.

[58] R. W. Damon and J. R. Eshbach, J. Phys. Chem. Solids, 19, 208 (1961).

[59] J. Jorzick, S. O. Demokritov, C. Mathieu, B. Hillebrands, B. Bartenlian, C. Chappert, F. Rousseaux, and A. N. Slavin *Phys.Rev.B.*, vol. 60, p. 15194, 1999.

[60] M. Bailleul, D. Olligs, C. Fermon, and S. O. Demokritov *Europhys. Lett.*, p. 741, 2001.